STUDY ON THE PERFORMANCE OF SEMICONDUCTOR THERMOELECTRIC GENERATOR SYSTEM DRIVEN BY SALT GRADIENT SOLAR POND

Hao Ma, Hua Wang ∗

School of Mechanical and Power Engineering, Henan Polytechnic University,

2001 Century Avenue, Jiaozuo 454003, Henan, PR China

wanghua@hpu.edu.cn

The performance of a semiconductor thermoelectric generator system based on the Lower Convective Zone of a salt gradient solar pond and ambient has been studied numerically and experimentally. According to the numerically solar pond temperature development results, the temperature differential range of the thermoelectric generator system ranges from 14 to 36°C. The numerically results show that, with a load resistance of 2Ω for each thermoelectric generator unit, among the four days selected, the temperature difference power generation system had the highest output power and conversion efficiency of 4.66W and 2.95%, respectively, on October 1st. Based on the numerical results of the temperature developments salt gradient solar pond, thermoelectric power generation experimental setup which operates under adjustable hot and cold reservoirs has been constructed. The experimental device runs under the conditions that the cold side temperatures of thermoelectric generator are 10°C, 24°C, and 38°C, and the load resistance is 10Ω. The maximum current is 0.149 A, 0.159 A and 0.124 A, the maximum voltage is 1.49 V, 1.59 V and 1.24 V, respectively. The average deviations between the theoretical results and the experimental results of the current and voltage generated by the power generation system are 0.026 A, 0.023 A, 0.012 A and 0.26 V, 0.23 V, 0.12 V, respectively.

Key words: salt gradient solar pond; semiconductor thermoelectric generator; thermoelectric conversion; power generation

1. Introduction

The salt gradient solar pond (SGSP) represents a saline reservoir with a distinctive gradient in salt concentration, designed to absorb solar radiation and store it as thermal energy [1]. It consists of three zones: the Upper Convective Zone (UCZ), the Non-Convective Zone (NCZ), and the Lower Convective Zone (LCZ) [2]. Recognized for its commendable economic viability and thermal efficiency, the SGSP is frequently employed as a low-temperature hot source for various applications. including power generation, heating,

∗ Corresponding author: Wang, Hua
Email: wanghua@hpu.edu.cn

hydrogen production, and seawater desalination [3, 4].

Presently, the utilization of the SGSP is mainly around heat supply applications [5]. However, in recent years, researchers have increasingly directed their focus toward the amalgamation of the SGSP with power generation equipment, aiming to facilitate thermoelectric conversion[6].

Thermoelectric generators (TEGs) are environment-friendly generators without mechanical parts, they have the advantage that they do not produce noise and can be manufactured in the desired size [7]. The structure of TEGs is usually that multiple semiconductor PN thermocouple units are arranged in series between ceramic substrates. TEGs can convert thermal energy into electrical energy under certain conditions, and the process mainly involves important thermoelectric effects such as the Seebeck effect. The thermoelectric effect-based technology for power generation from SGSP involves the integration of the SGSP with TEG. This combination exploits the thermoelectric conversion effect to generate electricity. Ding et al. [8] developed a compact power generation experimental setup utilizing the heat within the LCZ of SGSP for thermoelectric conversion. Operating at LCZ temperatures ranging from 40-80°C, the experimental setup demonstrated conversion efficiencies between 0.37% and 0.68%. In addition to the integration of the SGSP with TEGs, Goswami et al. [9]adopted a similar strategy, combining the SGSP with heat pipes for thermoelectric conversion under actual weather conditions. Results revealed a maximum ΔT of 23.57°C, corresponding to an open-circuit voltage of 1.435 V. Yakut et al. [10]established a new type of hot spot generator system and studied its performance. The experimental results show that the maximum open circuit voltage provided by the experimental device is 7.52 V, the maximum short circuit current is 1.392 A, and the maximum output power is 5.236 W.

The present study investigates the performance of TEG system. The main contents of this paper are as follows：

(1) Firstly, the temperature developments of SGSP have been simulated numerically, and the performance of the TEG system calculated accordingly.
(2) Secondly, an experimental equipment for the thermoelectric power generation is designed and constructed. Based on the theoretical results, a series of experiments were carried out under different temperature of hot and cold reservoirs.
(3) Finally, the experimental and theoretical results have been compared and discussed. The present study provides the theoretical and technical support for the practical application of TEG system.

2. Numerical model

2.1 Initial conditions

In this study, a one-dimension transient numerical heat transfer model for a SGSP with a surface area of 50 m × 50 m and a depth of 2 m is established. The coastal city of Tianjin, China (39°50′N), is chosen as the operational location for the SGSP. The UCZ of SGSP is a freshwater layer with a thickness of 0.2 m; The density range of NCZ is 1000-1200kg / m^3 (The saline water density increases by 2 kg/m^3 for each 0.01 m increase in the thickness of the

NCZ.), with a thickness of 1.0m; The density of LCZ is 1200kg / m^3 and the thickness is 0.8m. The internal region of the SGSP is discretized into 200 imaginary layers, with a spatial step size of Δx = 0.01m and a time step size of Δt = 0.05h. The load resistance of each TEG unit is 2Ω.

In the actual operation process, the temperature and salt concentration changes of SGSP are very complex, and semiconductor thermoelectric materials have temperature dependence. To simplify the problem analysis, some reasonable assumptions are made in the numerical simulation process. The assumptions are as follows:

(1) Given the expansive surface area of the SGSP and the presence of insulating material on the sidewalls, a one-dimensional heat transfer model is applied. This focuses on the temperature variation along the depth direction, assuming relatively uniform internal state parameters in the horizontal plane. The heat loss on the side wall of the solar pond has been neglected.

(2) For TEG, the temperature distribution is uniform at both ends of the module, the operating state is steady state, each PN junction is of the same size, and the heat conduction is only along the height direction of the PN junction.

(3) Disregarding the contact thermal resistance, the temperatures at the cold and hot ends of the TEG are the ambient temperature and the temperature of the LCZ, respectively.

(4) It is assumed that there is no heat loss between the heat source and the TEG, and the influence of the Thomson effect is not considered. The Seebeck coefficient, electrical conductivity and thermal conductivity of TEG are functions of temperature and change with temperature.

2.2 Solar radiation and ambient temperature

The transient equation for one-dimensional heat transfer in the SGSP numerical model is obtained from the governing equation:

$$\frac{\partial T}{\partial t}=\frac{\partial}{\partial y}(k\frac{\partial T}{\partial y})+\frac{\dot{q}(y)}{\rho C_{\mathrm{P}}} \tag{1}$$

where, $\dot{q}(y)$ represents the heat generation rate per unit volume at depth y within the SGSP, W/m^3. It is connected to the extinction coefficient μ [11, 12]. The value of μ ranges between 0 and 1. The value of μ ranges from 0-1, μ=0 indicates the state of absolute light transmission, the water in the solar pond is absolutely clarified, no absorption of light; Conversely, μ=1 indicates that the water is turbid, cannot make the light through, that is, all the light incident on the solar pond is absorbed by the water. In practice, the turbidity of the water is generally between the two.

$$\dot{q}(y)=0.6\cdot q(n_0,t_0)\cdot\mu\cdot exp(-\mu y) \tag{2}$$

where $q(n_0,t_0)$ is the solar radiation intensity incident on the SGSP surface [13], W/m^2:

$$\mathrm{q}(n_0,t_0)=\frac{24\times3.6G_{\mathrm{sc}}}{\pi}\left[1+0.033\cos(\frac{2\pi n_0}{365})\right]\times(\cos\varphi\cos\delta\sin\omega_{\mathrm{s}}+\omega_s\sin\varphi\sin\delta)\times\left[a_0+b_0\frac{n_i}{N}\right] \tag{3}$$

where, G_{sc} is the solar constant, G_{sc} =1353 W/m^2, while a_0 and b_0 are climate-related correction factors with values of 0.248 and 0.752, respectively[14]. n_i/N represents the

sunshine percentage, indicating the ratio of actual sunshine hours to astronomical sunshine hours, where N is derived from local climate data and is calculated using the formula [15]:

$$N=\frac{2}{15}\times\frac{180\cos(-\tan\delta\tan\varphi)}{\pi} \tag{4}$$

where, φ denotes the latitude, δ is the solar declination angle, and ω is the hour angle, rad, which are expressed as:

$$\delta=\frac{23.45\pi}{180}\sin\left(\frac{360(284+n_0)}{365.25}\right) \tag{5}$$

$$\omega=\frac{2\pi(t_0-12)}{24} \tag{6}$$

where, n is the number of days from January 1st, and t_0 represents time in a 24-hour format. The upper surface temperature assumption in UCZ aligns with the ambient temperature T_a, which can be determined using the empirical formula (7) [14]:

$$T_a(t)=T_{aver}+0.489\Delta T_1\cos\frac{\pi(t_0-15.05)}{12} \tag{7}$$

where, T_{aver} corresponds to the monthly average daily temperature, obtainable from local meteorological services, ℃; ΔT_1 signifies the daily temperature difference, ℃.

2.3 Saline water properties

The specific heat capacity of saline water within SGSP is a function of salinity, and the density and thermal conductivity of saline water is a function of salinity and temperature, where C is the heat capacity of the saline water, kJ/ (kg· K); c is the salinity of the saline water, kg/m^3; ρ is the density of the saline water, kg/m^3; and k is the thermal conductivity of the saline water, W/(m·K). The relationship between these parameters is expressed by the equation[16]：

$$C=(4180-4.396c+0.0048c^2)/1000 \tag{8}$$

$$\rho=998+0.65c-0.4(T-20) \tag{9}$$

$$k(c,T)=3.6\times[0.5553-8.13\times10^{-4}c+8\times10^{-4}(T-293)] \tag{10}$$

2.4 Performance of the thermoelectric generator system

The open-circuit voltage generated by the TEG is given by [17]:

$$E=\alpha(T_h-T_c) \tag{11}$$

where, E is the open-circuit voltage, V; α is the Seebeck coefficient of the thermoelectric material, V/K; T_h and T_c are the hot side and cold side temperatures of the TEG, respectively, K.

The energy balance equations for the TEG are established as follows [17]:

$$Q_h=n\left[\alpha IT_h+K(T_h-T_c)-\frac{1}{2}I^2R_{in}\right] \tag{12}$$

$$Q_c=n\left[\alpha IT_c+K(T_h-T_c)+\frac{1}{2}I^2R_{in}\right] \tag{13}$$

where, Q_h and Q_c represent the heat absorbed from the hot side and released to the cold side

by the TEG, W; n is the number of PN junctions; K is the thermal conductivity of the thermoelectric material, W/K; R_{in} is the internal resistance of the TEG, Ω; I is the current in the circuit, A.

The current in the circuit and the load voltage are given by [18]:

$$I=\frac{E}{R_L+R_{in}} \tag{14}$$

$$U=(\frac{E}{R_L+R_{in}})R_L \tag{15}$$

where, U is the voltage of the load, V; R_L is the load resistor, Ω.

The output power and conversion efficiency of the thermoelectric power generation module are expressed as [19]:

$$P=UI=(\frac{E}{R_L+R_{in}})^2R_L \tag{16}$$

$$\eta=\frac{P}{Q_h} \tag{17}$$

where, P is the output power of the load, W; η is the conversion efficiency of TEG, %.

3. Structure and working principle of experimental setup

The thermoelectric power generation experimental setup built in this study, is composed of three integral modules: as shown in Fig.1, the hot-side module, the TEG module and the cold-side module. Hot-side module consists of hot reservoir, water bath, peristaltic pump; cold-side module consists of a cold reservoir, water valve; the TEG module consists of five TEGs connected in series, forming a closed-circuit with an electronic load and a digital multimeter. The specification of the TEGs is shown in Tab. 1; temperature recorder is used to record the temperature of the hot and cold reservoirs. To minimize contact thermal resistance between the TEGs and the walls of the hot and cold reservoirs, a layer less than 1mm of thermal grease is applied to the surface of the TEGs. The thermal conductivity of the thermal grease is 14.3 W/m·K.

The experimental setup employs the hot-side module to simulate the LCZ of a SGSP, while the cold-side module replicates ambient temperatures during various seasons; Situated between the hot-side module and cold-side module, the TEGs, in conjunction with a multimeter and electronic load, form a closed-circuit. This circuit perform thermoelectric conversion based on the Seebeck effect, thereby generating electrical energy. The electronic load is utilized for collecting load output voltage and load output power, with the data transmitted to a computer. A temperature recorder is employed to document temperature variations in the cold and hot reservoirs.

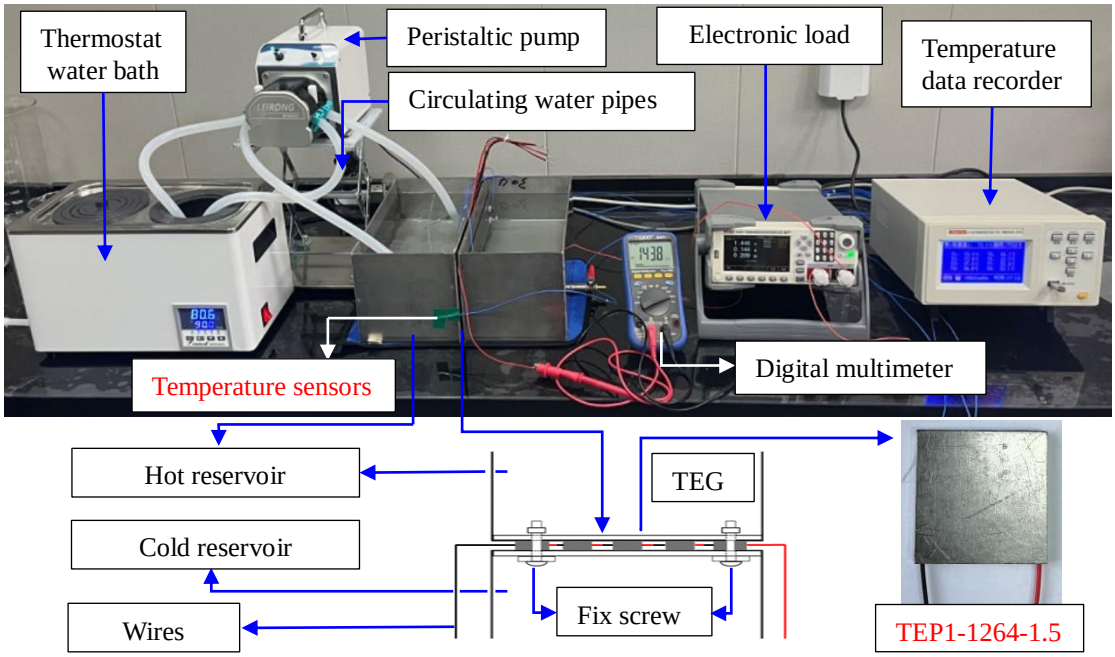

Fig.1 Thermoelectric power generation experimental setup

Tab.1 Specification of TEG

	Value
Type of TEG	TEP1 -1264-1.5
Thermoelectric material	Bi_2Te_3
Size of TEG (mm)	40×40×3.9
The number of PN junctions	126
The size of PN junctions (mm)	1.5×1.5×1.3
Matched load output power (W)	7.3
Resistance (Ω)	1.3-1.8

4. Numerical results and discussion

4.1 Temperature development of salt gradient solar pond

The efficiency of the TEG system driven by SGSP is mainly affected by the ΔT between the cold and hot reservoirs. Consequently, this study places a particular emphasis on monitoring both the ambient temperature and the LCZ temperature of SGSP. Fig. 2 presents the simulated variations in ambient temperature and the LCZ temperature during the operational phase of the SGSP. The SGSP commenced formal operations on April 1st (Day 91) and continued for a duration of 365 days. As illustrated in Fig. 2, during the initial stages of operation, when the SGSP had just commenced, the LCZ temperature closely tracked the ambient temperature, both fluctuate around 7°C. With the progressive operation of the SGSP, the LCZ temperature gradually increased. The LCZ temperature surpassed the ambient temperature from the 6th day. After operated 135 days (August 14th), the average temperature of the LCZ reached its peak of 67.8°C, while the ambient temperature stood at 33.7°C,

resulting in a temperature differential of 34.1°C. Notably, the LCZ temperature shows a characteristic of uniform variation with the increasing operational time, rather than showing significant fluctuations in response to changes in ambient temperature.

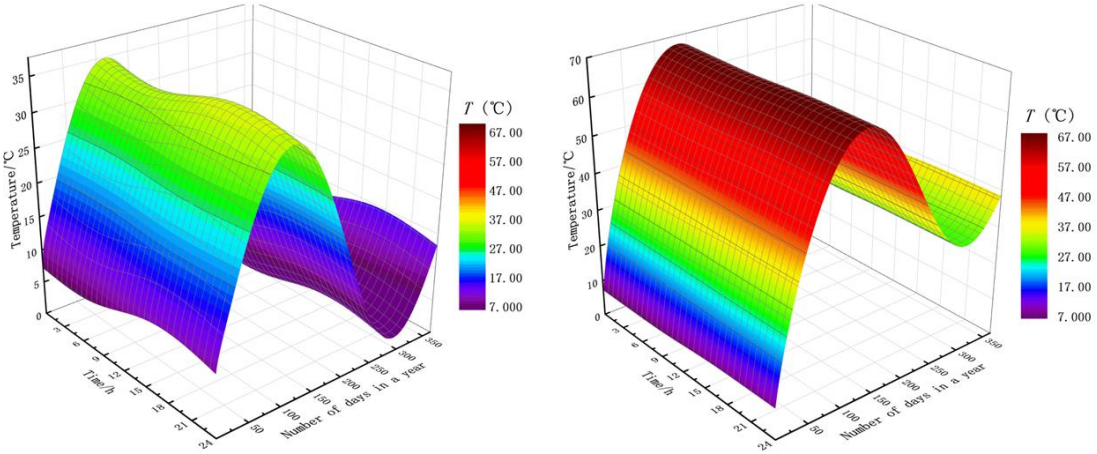

(a) The ambient temperature (b) The LCZ temperature

Fig.2 Temperature development of the SGSP during one year of operation

Fig. 3 illustrates substantial fluctuations in ambient temperature on all four typical days in a year, demonstrating a characteristic pattern of initial decrease followed by an increase, where June 1st (Day 152), August 1st (Day 213), October 1st (Day 274), and December 1st (Day 335) are used to represent the four seasons of spring, summer, autumn, and winter in a year, respectively. In contrast, the temperature variations within SGSP, especially in LCZ, shows a comparatively smaller variation. The average LCZ temperatures on these four days are 51°C, 67°C, 60°C, and 39°C, and August 1st has the highest temperature. Similarly, the average temperature differentials of LCZ and ambient on these days are 23°C, 32°C, 37°C and 33°C, with October 1st exhibiting the highest average temperature differential.

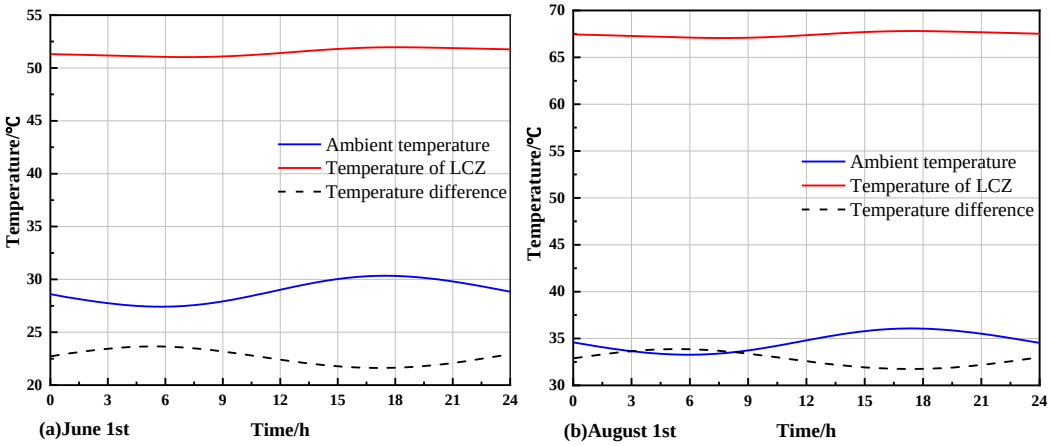

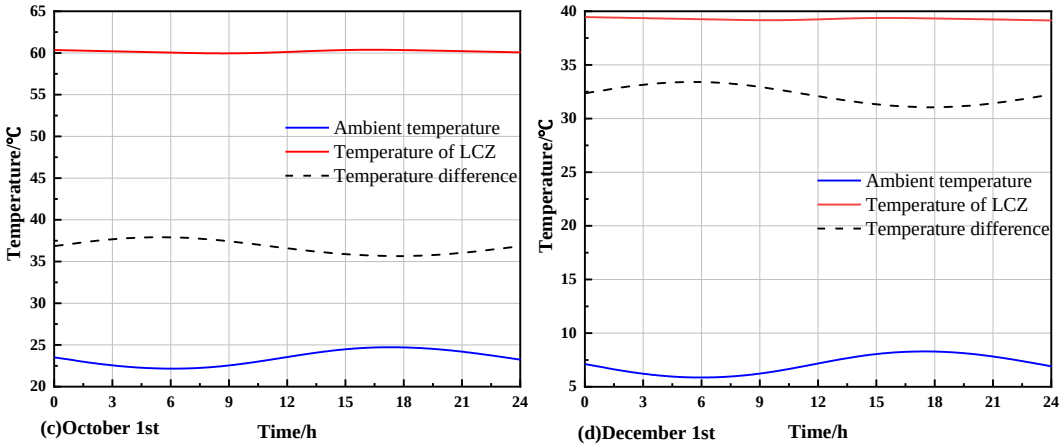

Fig.3 Temperature development in solar ponds on four dates

The above analyses reveal that throughout the year-long operational cycle, the temperature within the LCZ of the SGSP undergoes even and gradual variation over time. Remarkably, the temperature changes within a single day remain below 1°C, affirming the SGSP's status as a dependable and stable hot reservoir. As a stable heat source, the SGSP can provide an average heat source temperature of nearly 40°C or more throughout the year; in summer, autumn and winter, the ΔT between the LCZ and the environment is more than 30°C, and only in the spring is the ΔT lower, but the ΔT in the spring is also increased in the actual multi-year operation situation.

4.2 Performance of the thermoelectric generator system

In the numerical calculation, SGSP was applied for the TEG system after it operated for 30 days (May 1st) with a rather stable state. Fig. 4 depicts the variation in the performance of the TEG system on June 1st, August 1st, October 1st, and December 1st, utilizing the SGSP as a constant-temperature hot reservoir. As illustrated in Fig.4, the performance trends of the TEG system on these selected days are all increasing and then decreasing, all reaching a maximum at around 3 a.m. and a minimum at around 14 p.m. The performance of the TEG system on each of these selected days is shown in Fig. 4. This is because the temperature difference between the LCZ and the environment is maximum around 3 a.m., so the current, voltage and output power generated by the power generation system reach the maximum value. Similarly, the temperature difference between the LCZ and the environment is minimum around 14 p.m., so the current, voltage and output power achieve minimum values. The maximum currents generated in the four days were 0.481A, 0.659A, 0.744A and 0.686A, and the maximum voltages were 4.81V, 6.59V, 7.44V and 6.86V, respectively. For all four days, the pinnacle of output power is reached at 3 a.m., registering values of 1.80W, 3.61W, 4.66W, and 3.86W, corresponding to thermoelectric efficiencies of 1.38%, 1.90%, 2.95%, and 2.07%, respectively.

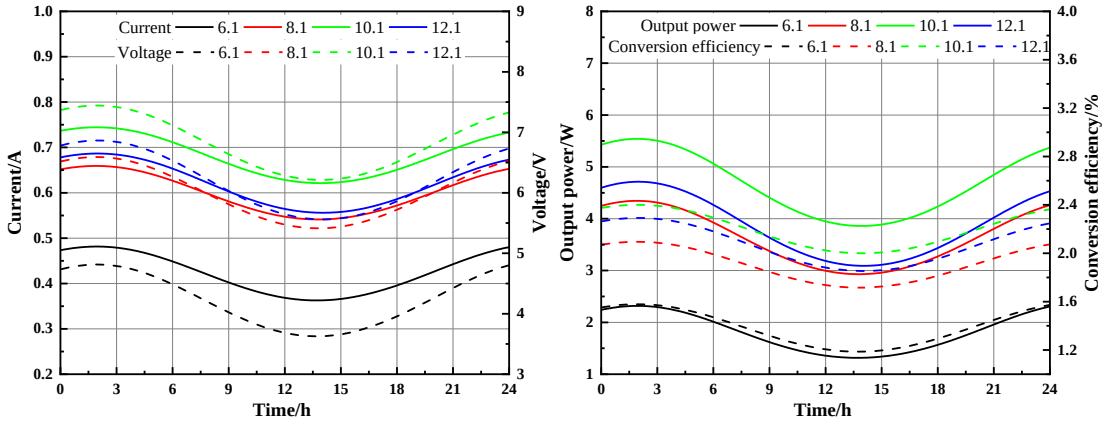

(a) The current and voltage values (b) The output power and efficiency

Fig. 4 Performance of thermoelectric generators on four dates

The above analysis indicates that the primary reliance of current and voltage output from the TEG system on the ΔT between the LCZ of the SGSP and the ambient environment. However, the temperature of the cold and hot ends of the TEG will have an effect on it as well. On both August 1st and December 1st, where the average temperature differentials between the LCZ and the environment differ by approximately 1°C, the resulting electrical output from the TEG system was similar, but the thermoelectric conversion efficiency on 1st December was slightly higher than that on 1st August. The temperature at the hot end of the thermoelectric generator is lower on 1st December than on August 1st, and from equations (12) (16) and (17), the output power of the TEG system is lower on December 1st than on August 1st, and the thermoelectric conversion efficiency is slightly higher on December 1st than on August 1st.

5. Experimental results and discussion

Based on the numerical studies, a thermoelectric power generation experimental setup was established. The cold side of TEG (T_c) of the experimental setup is used to simulate the average ambient temperature, and the hot side of TEG (T_h) is used to simulate the LCZ temperature. The ΔT between the hot and cold reservoir is used to drive the TEG to generate electricity. In order to simulate the ambient temperature of the four seasons in one year (the average ambient temperature in spring and autumn is 24 °C, 38 °C in summer and 10 °C in winter), the T_c of the experimental setup are 24 °C, 38 °C, 24 °C and 10 °C respectively, and the ΔT varies between 11 °C and 38 °C. Specifically, the experimental setup was operated under constant temperature conditions for the cold reservoir, with temperatures set at 10°C, 24°C, and 38°C, denoted as Case A, Case B, and Case C, respectively.

5.1 Performance of the experimental setup

Fig. 5 depicts the current variation produced by the experimental setup under different temperature differences. As can be seen in Fig. 5, the current, voltage and output power increase with the temperature difference under the three operating conditions; the current,

voltage and output power produced by the generation system are higher under Case A than the other two cases; and the current and voltage produced by the generation system are close to each other under Case B and Case C conditions. In three cases, the maximum current is 0.149 A, 0.159 A and 0.124 A, the maximum voltage is 1.49 V, 1.59 V and 1.24 V, and the maximum output power is 0.223 W, 0.254 W and 0.154 W, respectively. The experimental results show that the greater the temperature difference between the cold and heat sources, the greater the current, voltage and output power.

This is because when the ΔT increases, the open-circuit voltage E increases according to eq. (11)(16), the current and output power increases with the increase of open-circuit voltage under the condition that the load resistance remains unchanged; under the condition that the ΔT is the same, the temperature of the cold and hot reservoirs is different, and the current generated by the TEG is different. This is due to the thermoelectric figure of merit will change with the change of temperature[20], so the current generated by TEG is different in the same ΔT and different temperature ranges.

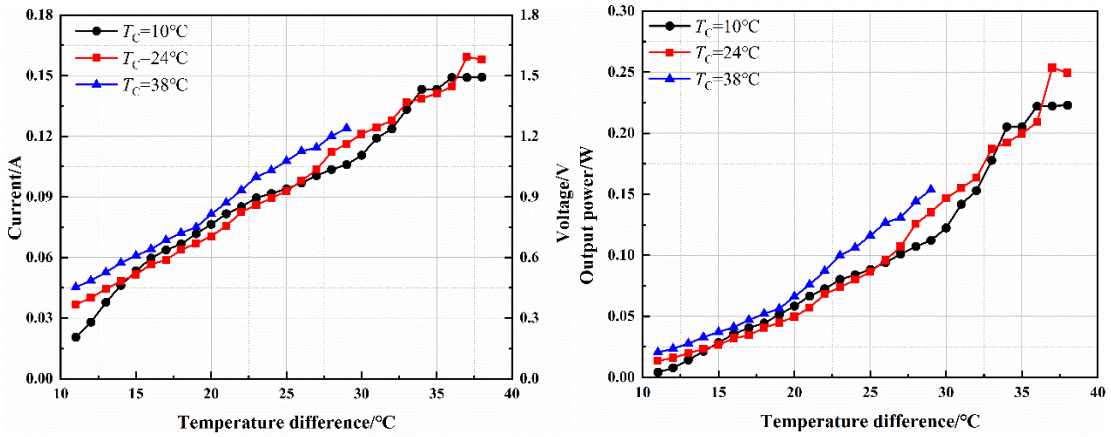

(a) The current and voltage values (b) The output power values

Fig. 5 The current generated by the thermoelectric power generation experimental setup

5.2 Comparative analysis of experimental and theoretical results

As depicted in Fig. 6, a comparative analysis between experimental and theoretical results reveals a consistent trend where the experimental outcomes under all three conditions consistently fall below their simulated counterparts. The average deviation of the experimental results from the theoretical calculations for the current and voltage generated by the power generation system for the three cases were 0.026A, 0.023A, 0.012A and 0.26V, 0.23V, 0.12V, respectively.

It can be ascribed to several contributing factors for the deviations between experiment and numeration. Firstly, the numerical model of the SGSP, characterized by a stable temperature due to the large volume, while the experimental setup employs comparatively smaller size chambers for the high and low- temperature hot reservoirs. Although these maintain stable water temperatures internally, the inherent thermal gradient across the steel walls introduces a disparity between the actual temperature of the TEG surface and the temperature of the hot reservoir. Consequently, theoretical results tend to surpass the corresponding experimental outcomes; In the process of theoretical simulation, the current

and voltage generated by the TEG are calculated according to a certain theoretical formula. In the experiment, the TEG needs to be connected in series, and the welding of the line will increase the internal resistance, so that the theoretical results are greater than the experimental results; Because the figure of merit of the thermoelectric material is closely related to the temperature, in most cases the figure of merit will increase with the increase of the temperature, and the larger the figure of merit is, the better the thermoelectric conversion performance of the material is [17]. The theoretical value of the thermoelectric material figure of merit in the low-temperature-difference range is about 1[21, 22], and we speculate that the higher the temperature at the ends of the TEG, the closer the experimental value of the thermoelectric material figure of merit is to the theoretical value. Among three cases, the temperature limitations range of Case A is lowest, leads to the smallest value of figure of merit, and the largest deviation of the experimental results from the theoretical results, while Case C has the highest temperature limitations range, the largest value of figure of merit, and the smallest deviation of the experimental results from the theoretical results. All the above reasons lead to some deviation of the experimental results from the simulation results.

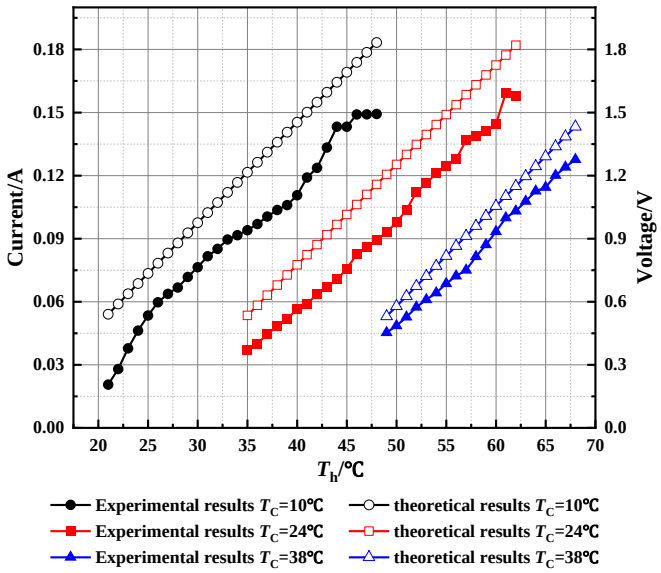

Fig.6 Comparison of experimental results and theoretical results

6. Conclusion

In this study, the numerical model of TEG system driven by SGSP and the thermoelectric power generation experimental setup are established. The results show that:

(1) In the numerical simulation, the current generated by the power generation system in the four days is 0.481A, 0.659A, 0.744A, 0.686A, respectively; the voltage is 4.81V, 6.59V, 7.44V, 6.86V, respectively; the output power is 1.80W, 3.61W, 4.66W, 3.86W; the conversion efficiency is 1.38%, 1.90%, 2.95%, 2.07%. 2.95%, 2.07%.

(2) Under the experimental conditions of this study, the generated current and voltage from the TEG primarily depend on the ΔT between the LCZ temperature and the ambient temperature, and the current increases with the increase of the ΔT; it is also influenced by the actual temperatures at both ends of the TEGs, and the current increases with the

increase of the temperatures.

(3) The setup under different temperatures of the cold reservoir (10℃, 24℃, and 38℃), a ΔT ranging from 11 to 38℃, and a load resistance of 10Ω. The maximum current is 0.149 A, 0.159 A and 0.124 A, the maximum voltage is 1.49 V, 1.59 V and 1.24 V, and the maximum output power is 0.223 W, 0.254 W and 0.154 W, respectively. The average deviation of the experimental results from the theoretical calculations for the current and voltage for the three cases were 0.026A, 0.023A, 0.012A and 0.26V, 0.23V, 0.12V, respectively.

(4) Theoretical results are higher than the experimental results, since there exists heat loss for the hot reservoir, which makes the hot side temperature of the TEG different from the actual temperature of the heat reservoir; the welding of the circuit increases the internal resistance of the experimental setup; the figure of merit of the thermoelectric material during the experiment is affected by temperature and other factors and is less than the theoretical value.

Acknowledgements

This work has been carried out with the support of Science and Technology Research Project of Henan Province (232102321088).

Reference

[1] SHAH N-U-H, ARSHAD A, KHOSA AZHAR A, et al. Thermal analysis of a mini solar pond of small surface area while extracting heat from lower convective layer [J]. THERMAL SCIENCE,2019, 23(2A), pp. 763-776, DOI: https://doi.org/10.2298/TSCI170129166S

[2] SOGUKPINAR H, BOZKURT I, KARAKILCIK M. Performance comparison of aboveground and underground solar ponds [J]. THERMAL SCIENCE, 2018, 22(2), pp. 953-961, DOI: https://doi.org/10.2298/TSCI160613269S.

[3] EL-SEBAII A A, RAMADAN M R I, ABOUL-ENEIN S, et al. History of the solar ponds: A review study [J]. Renewable and Sustainable Energy Reviews, 2011, 15(6), pp. 3319-25，DOI: https://doi.org/10.1016/j.rser.2011.04.008.

[4] PRAJAPATI S, MEHTA N, YADAV S. An overview of factors affecting salt gradient solar ponds [J]. Materials Today: Proceedings, 2022, 56, pp. 2742-52,DOI: https://doi.org/10.1016/j.matpr.2021.09.538.

[5] BOZKURT I. The investigation of using phase change material for solar pond insulation [J]. THERMAL SCIENCE, 2022, 26(2C): pp.1799-1808, DOI:https://doi.org/10.2298/TSCI210309185B.

[6] DING L C, AKBARZADEH A, SINGH B, et al. Feasibility of electrical power generation using thermoelectric modules via solar pond heat extraction [J]. Energy Conversion and Management, 2017, 135,pp. 74-83, DOI: https://doi.org/10.1016/j.enconman.2016.12.069.

[7] ATALAY T, YAKUT Y, KöYSAL Y, et al. Experimental and Thermal Analysis of Solar Thermoelectric System Performance Incorporated with Solar Tracker [J]. International Journal of Precision Engineering and Manufacturing-Green Technology, 2021, 9(2),pp. 587-602, DOI:https://doi.org/10.1016/j.applthermaleng.2023.121834.

[8] DING L C, AKBARZADEH A, DATE A, et al. Passive small scale electric power generation using thermoelectric cells in solar pond [J]. Energy, 2016, 117,pp. 149-65, DOI:https://doi.org/10.1016/j.energy.2016.10.085.

[9] GOSWAMI R, DAS R. Experimental analysis of a novel solar pond driven thermoelectric energy system [J]. Journal of Energy Resources Technology, 2020, 142(12), DOI: https://doi.org/10.1016/j.ijheatmasstransfer.2020.120844.

[10] YAKUT Y, ÖZBEKTAŞ S, KöYSAL Y, et al. Experımental investıgatıon and mathematıcal modelıng of a novel solar thermoelectrıc generator incorporated with thermal condensing system [J]. Applied Thermal Engineering, 2024, 236, DOI: https://doi.org/10.1016/j.applthermaleng.2023.121834.

[11] MANSOUR R B, NGUYEN C T, GALANIS N. Transient heat and mass transfer and long-term stability of a salt-gradient solar pond [J]. Mechanics Research Communications, 2006, 33(2), pp. 233-49, DOI: https://doi.org/10.1016/j.mechrescom.2005.06.005.

[12] GIESTAS M, PINA H, JOYCE A. The influence of radiation absorption on solar pond stability [J]. International Journal of Heat and Mass Transfer, 1996, 39(18), pp.3873-85, DOI: https://doi.org/10.1016/0017-9310(96)00052-X.

[13] WANG H, WU Q, MEI Y, et al. A study on exergetic performance of using porous media in the salt gradient solar pond [J]. Applied Thermal Engineering, 2018, 136,pp. 301-8, DOI: https://doi.org/10.1016/j.applthermaleng.2018.03.025.

[14] H.F. Zhang, Solar Energy Thermal Application and Simulation, (Eds.: Y.C. Zhang), Xi'an Jiao Tong University Press Co., LTD., Xi'an,China, 2012.

[15] WANG H, ZOU J, CORTINA J L, et al. Experimental and theoretical study on temperature distribution of adding coal cinder to bottom of salt gradient solar pond [J]. Solar Energy, 2014, 110,pp.756-67, DOI: https://doi.org/10.1016/j.solener.2014.10.018.

[16] JAEFARZADEH M R. Thermal behavior of a small salinity-gradient solar pond with wall shading effect [J]. Solar Energy, 2004, 77(3),pp. 281-90, DOI: https://doi.org/10.1016/j.solener.2004.05.013.

[17] DING L C, AKBARZADEH A, DATE A. Performance and reliability of commercially available thermoelectric cells for power generation [J]. Applied Thermal Engineering, 2016, 102, pp.548-56,DOI: https://doi.org/10.1016/j.applthermaleng.2016.04.001.

[18] CHEN W-H, LIN Y-X, WANG X-D, et al. A comprehensive analysis of the performance of thermoelectric generators with constant and variable properties [J]. Applied Energy, 2019, 241,pp.11-24,DOI: https://doi.org/10.1016/j.apenergy.2019.02.083.

[19] LI K, GARRISON G, MOORE M, et a l. An expandable thermoelectric power generator and the experimental studies on power output [J]. International Journal of Heat and Mass Transfer, 2020, 160, DOI: https://doi.org/10.1016/j.ijheatmasstransfer.2020.120205.

[20] TAN G, ZHAO L-D, KANATZIDIS M G. Rationally Designing High-Performance Bulk Thermoelectric Materials [J]. Chemical Reviews, 2016, 116(19),pp. 12123-49, DOI: https://doi.org/10.1021/acs.chemrev.6b00255.

[21] MA Z, WEI J, SONG P, et al. Review of experimental approaches for improving zT of thermoelectric materials [J]. Materials Science in Semiconductor Processing, 2021, 121, DOI: https://doi.org/10.1016/j.mssp.2020.105303.

[22] CHEN Y, HOU X, MA C, et al. Review of Development Status of Bi2Te3-Based Semiconductor Thermoelectric Power Generation [J]. Advances in Materials Science and Engineering, 2018, pp.1-9,DOI: |https://doi.org/10.1155/2018/1210562.

RECEIVED DATE: 04.03.2024.
DATE OF CORRECTED PAPER: 07.04.2024.
DATE OF ACCEPTED PAPER: 04.05.2024.